Asymmetric interfaces sandwiched between infinite-layer oxides and perovskite oxides

Xiaobing Chen [1,2] Shihao Zhang,[1,2] Banggui Liu [1,2] Fengxia Hu,[1,2,3] Baogen Shen,[1,2,3] and Jirong Sun [1,2,3,4,*]

[1]*Beijing National Laboratory for Condensed Matter Physics & Institute of Physics, Chinese Academy of Sciences, Beijing 100190, People's Republic of China*
[2]*School of Physical Sciences, University of Chinese Academy of Sciences, Beijing 100049, People's Republic of China*
[3]*Songshan Lake Materials Laboratory, Dongguan, Guangdong 523808, People's Republic of China*
[4]*Spintronics Institute, University of Jinan, Jinan, Shandong 250022, People's Republic of China*

Asymmetric heterointerfaces that bridge two nonisostructural oxides provide valuable opportunities for novel emergent phenomena that may be unavailable for symmetric interfaces. Here we present a theoretical investigation on three different asymmetric interfaces consisting of the infinite-layer nickelate $LaNiO_2$ and the perovskite manganite $LaMnO_3$ (type A, B and C). An alternative crystal geometry, pyramid, is introduced when the planar-type $LaNiO_2$ and the $LaMnO_3$ are jointed at the interface, resulting in strong charge and orbital reconstruction. For type A interface, the magnetic moment per Mn ion has increased by 10% due to the replacement of MnO_6 by MnO_5. For type B interface, in contrast, the magnetic moment grew by 26% for the interfacial Ni ions due to the strong charge transfer between center nickel and apical oxygen. For type C interface, only slightly enhanced MnO_6 distortions are observed and thus the change of charge and orbital occupancy are negligible. Our results demonstrated that an interface-selective orbital occupancy, where the Mn e_g orbital preferential occupation alternated from the out-of-plane $d_{3z^2-r^2}$ state at type A interface to nearly degenerate at type C interface and then to in-plane $d_{x^2-y^2}$ state at type B interface. The values of relative change of Mn e_g orbital occupancy are 15%, 2%, and −21%, respectively. The values of relative change at type A and B interface are larger than that achieved by strain ($\sim$5%) or symmetric interface design (10%). Therefore, interface reconstructions lead to unusual electronic properties, opening space for the advancement of oxide electronics.

I. INTRODUCTION

Atomic engineering of complex oxide interfaces is a powerful way to control the spin, charge, lattice and orbital degrees of freedom [1]. Particularly oxygen plays a pivotal role in manipulating such orbital degrees of freedom and has reveals many intriguing phenomena impossible in bulk material counterparts, such as the high-T_C superconductivity at the interface between $Nd_{0.8}Sr_{0.2}NiO_3$ and $SrTiO_3$ [2], the large orbital polarization in $SrCuO_2/LaNiO_3$ heterostructures [3], the perpendicular magnetic anisotropy at the interface of $LaCoO_{2.5}/La_{0.67}Sr_{0.33}MnO_3$ [4], and the covalent bonding at the $(Y,Ca)Ba_2Cu_3O_7$ and $La_{0.67}Ca_{0.33}MnO_3$ interface [5]. Therefore, asymmetric interfaces that bridge two nonisostructural oxides provide a wide space for the exploration for emergent phenomena [6].

Perovskite $LaMnO_3$ (LMO), the parent compound of the colossal magneto-resistance manganites [7], offers promising theoretical and experimental platforms to investigate the effect associated with orbital degree of freedom. The $3d^4$ configuration of Mn^{3+} in LMO contains a half occupied t_{2g} shell and a single electron occupied e_g orbital. The $LaNiO_2$ (LNO), which in bulk phase is orthorhombic ($P4/mmm$) with layers of Ni atoms in fourfold planar oxygen coordination

separated by interplanar bare La atoms [8]. The Ni ion in LNO has the same formal ionic configuration $3d^9$ as Cu does in isostructural $SrCuO_2$, the parent infinite-layer material of high-T_C superconductors. However, the $LaNiO_2$ is reported to be a nonmagnetic bad metal [9] whereas $SrCuO_2$ is an antiferromagnetic insulator.

Here we report an intriguing model system comprised of infinite-layer nickelate LNO and perovskite manganite LMO. Similar to the $SrCuO_2$ film [10], the NiO_2 planes in LNO can be either planar type (P-LNO) or chain type (C-LNO), parallel or perpendicular to film plane. As a result, we have three different LNO/LMO superlattices which have $NiO_2|La|MnO_2$, $NiO_2|LaO|MnO_2$ and $NiO|LaO|MnO_2$ interface configurations, respectively (see Fig. 3). The corresponding interfaces are denoted by type A, B, and C interfaces. Based on density functional theory (DFT) calculations, the magnetic ground state and the thermodynamic stability are determined. The MnO_5 (NiO_5) pyramid structure is induced at type A (B) interface, whereas the MnO_6 octahedron remain unchanged at type C interface, allowing us to selectively control the charge and orbital reconstruction. Also, the circumstance of interface Mn (Ni) ions changes, resulting in significant changes in valence state and magnetic moments. Finally, our results demonstrated how the infinite-layer structure can be utilized to induce an interface-selective orbital occupancy at Mn sites through oxygen sublattice modulation. The values of the relative change of e_g occupancy at type A and type B interface are both larger

*Correspondence author: jrsun@iphy.ac.cn

than that achieved by strain. All these results demonstrated the potential of oxygen coordination manipulation in the design of complex oxide interfaces.

II. COMPUTATIONAL DETAILS

DFT calculations within the projected augmented-wave method [11] as implemented in the Vienna *ab initio* simulation package [12,13] codes were used to investigate three superlattices. The generalized gradient approximation of Perdew-Burke-Ernzernhof modified for solids was adopted for exchange-correlation energy [14,15]. A 500-eV kinetic energy cutoff was found to achieve numerical convergence. We adopted k-point sets generated by $9 \times 9 \times 9$, $9 \times 9 \times 1$ and $9 \times 9 \times 3$ Monkhorst-Pack meshes for bulk LNO, LNO films and LNO/LMO superlattices, respectively. A vacuum of 15 Å was added only in LNO films to probe the evolution of structure transition. In the electronic structure calculations, we used dense k meshes of $13 \times 13 \times 13$, $13 \times 13 \times 1$ and $13 \times 13 \times 5$ for bulk LNO, LNO films and LNO/LMO superlattices, respectively. To study the effect of electron correlation, the DFT $+ U$ approach within the rotationally invariant Liechtenstein's formalism was performed with $U(\text{Mn})$ $= 3.5$ eV, $J(\text{Mn}) = 0.9$ eV, $U(\text{Ni}) = 5.0$ eV, $J(\text{Ni}) = 0.8$ eV for Mn and Ni $3d$ orbitals, respectively [16–18]. Atomic positions were optimized until the Hellman-Feynman force on each atom was smaller than 0.01 eV/Å and the electronic iteration was performed until the total energy change was smaller than 10^{-5} eV. A wide range of U from 1.0 to 7.0 eV for Ni $3d$ orbitals were also performed and we found the variation of U made a negligible contribution to the main conclusion of our work. Detailed results about the effect of U are presented in the Supplemental Material [19]. The corresponding chemical potentials are determined from total energy calculations of equilibrium bulk structures using the same setting. The in-plane lattice constants of superlattices were fixed to $a = 3.905$ Å, which corresponds to the value of bulk SrTiO$_3$. The in-plane $\sqrt{2}a \times \sqrt{2}a$ geometry was also adopted for the search of the magnetic ground state. Besides A-type antiferromagnetic (AFM), C-type AFM, G-type AFM and ferromagnetic (FM) order, we also checked all the possible linear combinations of these orders.

III. RESULTS AND DISCUSSION

A. Ideal polar thin films of LNO

First, we calculate the parent compound LNO. The magnetic ground state of the LNO film is found to be G-type AFM order when $U_{\text{Ni}} < 5$ eV and C-type AFM when $U_{\text{Ni}} \geqslant 5$ eV, in agreement with previous calculations [18,20]. The G-type AFM and C-type AFM are always energetically close when U_{Ni} varied from 1.0 to 7.0 eV as shown in Table S1 of the Supplemental Material [19], which induced the magnetic instability in LNO. Additionally, the self-doped hole effects from La $5d$ bands (shown in Fig. S3(a) [19]) are also likely responsible for the suppression of magnetism [18]. Therefore, the LNO behaves as a nonmagnetic bad metal experimentally rather than AFM insulator.
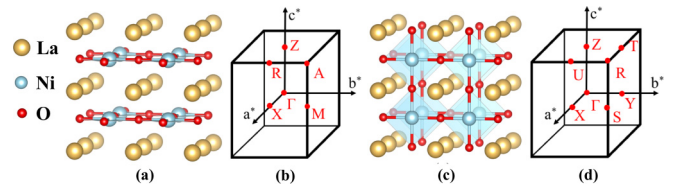

FIG. 1. Sketches of infinite-layer structure thin film with (a) planar-type LNO and (c) chain-type LNO, resulting in different oxygen sublattice and electrostatic potential. The primitive reciprocal lattice vectors and high-symmetry k points are indicated in the first Brillouin zones of (b) P-LNO and (d) C-LNO.

As stated before, LNO is isostructural to SrCuO$_2$. Thus, we have two types of structures when LNO is grown on a perovskite substrate, e.g., SrTiO$_3$. The planar-type structure is composed of positively charged La^{3+} and negatively charged NiO3- 2, while the chain-type structure comprised of less positively charged LaO^{1+} and negatively charged NiO^{1-}, at the cost of lattice strain [see in Figs. 1(a) and 1(c)]. The competition between strain and electrostatic field will affect interface stability, so we calculate the P-LNO and C-LNO grown on different substrates. The in-plane lattice constants are fixed at the equilibrium values of various substrates, including the LaAlO$_3$, (LaAlO$_3$)$_{0.3}$(SrAl$_{0.5}$Ta$_{0.5}$O$_3$)$_{0.7}$ (LSAT), SrTiO$_3$ and KTaO$_3$, and the corresponding lattice constants are 3.791, 3.868, 3.905,and 3.989 Å, respectively.

To find the critical thickness of thin films, the energy difference $\Delta E = E^{\text{chain}}$-$E^{\text{planar}}$ as a function of thickness d is shown in Fig. 2(a). ΔE depends strongly on both lattice strain and film thickness. Since the P-LNO and C-LNO share the same stoichiometry, the sign of ΔE is a direct indication of their relative stability under different strains. Below the critical thickness, the C-LNO films are energetically favorable, e.g., C-LNO films are favorable when the film thickness is below 2 uc on SrTiO$_3$ substrate. Above 2 uc, however, P-LNO films are more stable. With the decrease of in-plane lattice constant, the critical thickness gradually increases. This means that the C-LNO is more stable under compressive strain than under tensile strain.

Band structures of P-LNO and C-LNO grown on SrTiO$_3$ substrate are shown in Figs. 2(b) and 2(c). As shown in Fig. 2(b), the electronic structure shows an energy level splitting, consistent with the square planar crystal field and the strong hybridizations between Ni $3d$ and O $2p$ states. The nominal Ni^{1+} with $3d^9$ ionic configuration in P-LNO adopting square-planar coordination results in a high-lying nominally half-filled d$_{x^2-y^2}$ orbital. As shown in Fig. 2(c), the Ni^{1+} ions in C-LNO results in hole states comprised of d$_{3z^2-r^2}$ and d$_{x^2-y^2}$ orbital, similar with the previous report about the chain-type SrCuO$_2$ [21]. Through the integration of projected density of states and the analysis of crystal field based on coordination transformation [19], we conclude that the hole states of the d$_{3z^2-r^2}$ orbital and d$_{x^2-y^2}$ orbital have a ratio of 3:1. Obviously, the oxygen sublattice design has greatly modified the orbital occupation in LNO. Therefore, we propose that this structural transition can be effectively used for interface design by manipulating orbital degrees of freedom. To verify this assumption, we calculate three possible LNO/LMO superlattices via first-principles calculations.
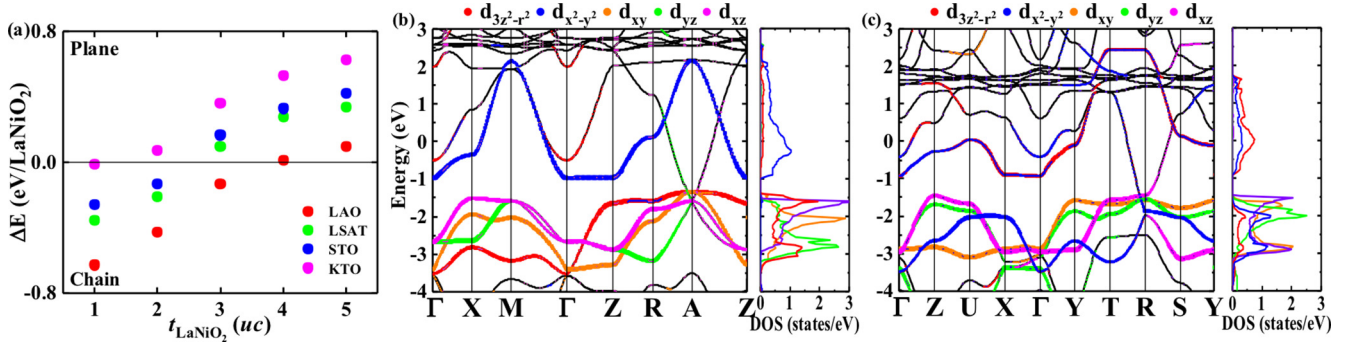
FIG. 2. (a) Total energy difference between planar- and chain-type LNO thin films as a function of the film thickness d. Band structure and the corresponding projected density of states of Ni $3d$ orbitals of (b) P-LNO and (c) C-LNO thin films on SrTiO$_3$ substrate.

B. Magnetic ground states

First, it is well-known that the magnetic ground state of bulk LMO is difficult to be captured by DFT calculations. Within the reported values of $U(\text{Mn}) = 3.5$ eV and $J(\text{Mn}) = 0.9$ eV [17], our calculations give an A-type AFM ground state, whose energy is lower than the FM state by 7.9 meV/Mn. When the LMO is strained on the SrTiO$_3$ substrate, our calculations give a FM ground state, whose energy is lower than the A-type AFM state by 5.4 meV/Mn. In the following calculations, the U and J of Mn will be adopted as default.

To fulfill the effects of oxygen octahedra rotation and tilting, we construct three LaNiO$_2$/LaMnO$_3$ superlattices with different interfacial configurations as shown in Fig. 3, including the NiO$_2$|La|MnO$_2$ interface (type A), the NiO$_2$|LaO|MnO$_2$ interface (type B), and the NiO|LaO|MnO$_2$ interface (type C).

The magnetic ground states of three superlattices are determined. In brief, we denoted FM, A-type AFM, C-type AFM and G-type AFM order as F, A, C, and G in the hybrid magnetic order. For example, the C-F state is C-type AFM magnetic order in Ni layers but FM order in Mn layers. We find that the G-A, C-F and F magnetic orders are the magnetic ground states for type A, B and C interfaces, respectively. The detailed calculated total energy difference of different magnetic orders is summarized in Table I. The effect of U_{Ni} values is also considered and we find that the magnetic orders of the superlattices are independent of U_{Ni} [19].

Furthermore, we discussed the self-doping effect for three superlattices as shown in S3 [19]. No electron pockets of La $5d$ bands were observed in type B and C superlattices, meaning that the long-range magnetic order of LaNiO$_2$ in these two superlattices are stable. However, the long-range magnetic order of LaNiO$_2$ in type A superlattice will be suppressed as the itinerant La-$5d$ bands self-dope the Ni-$3d$ band, while the main conclusions at LMO side are unchanged in type A superlattice when the LNO is nonmagnetic.

C. Structural stability

In this section, the question about the relative stability of three LNO/LMO superlattices is addressed. Following the thermodynamic approach [22,23], we define the formation energy as

$$E_f(X) = \tfrac{1}{2}(E(X) - 4E(LMO) - 4E(LNO) - x\mu_O),$$

where $E(X)$ is the total energy of the corresponding supercell X, μ_O denotes the chemical potential of O relative to its value in the most stable elementary phase of O, i.e., O$_2$ (that is $2\mu_O = E_{\text{tot}}^{O_2}$, where $E_{\text{tot}}^{O_2} = -6.14$ eV). Here $x = -2, 2$ and 0 for type A, B, and C superlattices, respectively. A negative value of $E_f(X)$ indicates that X is synthesizable.

According to the computed value of the total energies in each superlattice, the formation energies $E_f^A = +3.50$ eV, $E_f^B = -3.64$ eV, $E_f^C = -0.46$ eV are obtained. Detailed calculations of formation energies are given in the Supplemental Material [19]. The negative formation energies of type B and type C superlattices indicated that they are thermodynamically
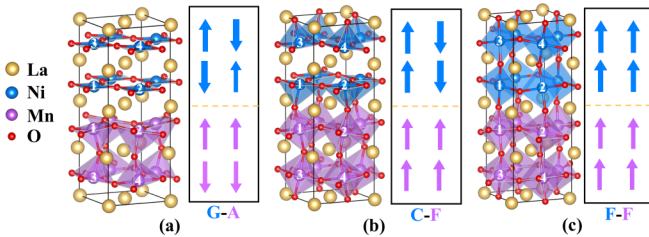

FIG. 3. Illustration of crystal structure of LNO/LMO superlattices with manipulated oxygen coordination: (a) NiO$_2$|La|MnO$_2$ interface (type A), (b) NiO|LaO|MnO$_2$ interface (type B) and (c) NiO|LaO|MnO$_2$ interface (type C). The B-site atoms are labeled from 1 to 4.

TABLE I. Summary of DFT energies (in units of meV per Ni-Mn combination) for three superlattices. The magnetic ground states of each superlattice are taken as the reference state for energy comparison. Here the A-A, F-F, A-F, C-F, G-F, C-A, G-A are hybrid magnetic states. The A-A (or F-F) state is A-AFM (or FM) order in both Ni's and Mn's layers, but coupled ferromagnetically (or antiferromagnetically) between Ni's and Mn's layers.

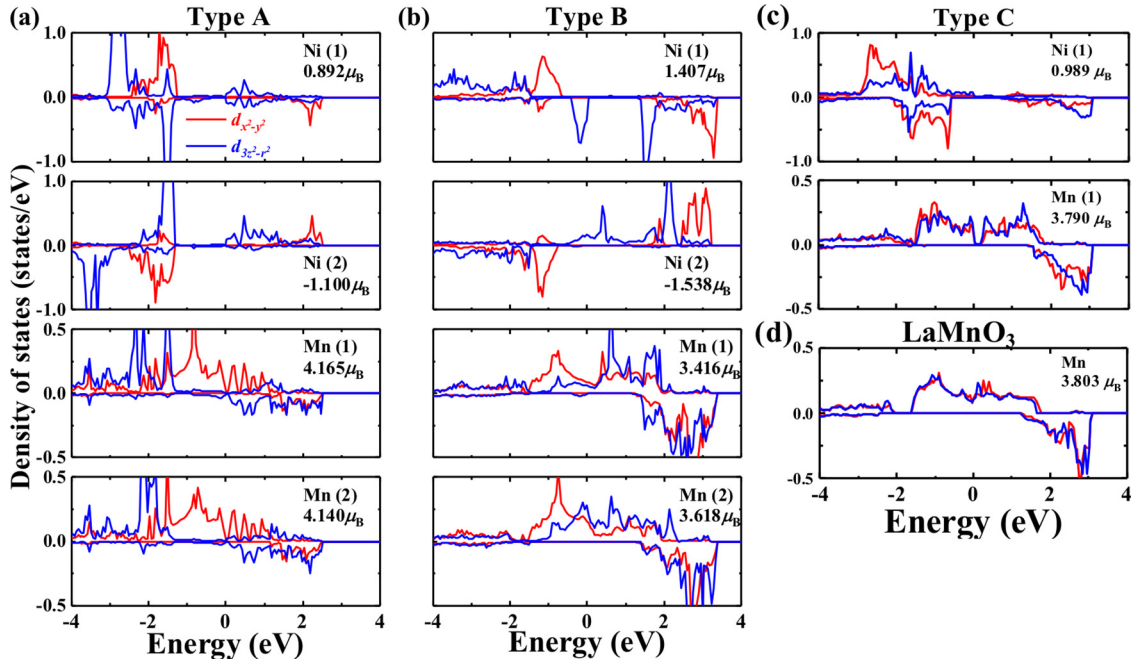| Type	F	A	C	G	A-A	F-F	A-F	C-F	G-F	C-A	G-A
A	68	111	100	139	48	150	115	33	34	4	0
B	91	196	203	309	227	55	190	0	97	8	109
C	0	45	104	126	2	52	20	15	10	16	12

FIG. 4. (a)–(c) The projected density of states of Ni and Mn e_g orbitals in three superlattices. The B-site atomic labels are the same as those denoted in Fig. 3 and the local magnetic moments are also indicated. (d) The projected density states of Mn e_g orbitals in bare LMO on STO.

stable. To compare their relative stability, their energy difference is defined as

$$\Delta E_f^{B-A} = E_f^B - E_f^A - 2\mu_O,$$

$$\Delta E_f^{C-B} = E_f^C - E_f^B + \mu_O.$$

For the three interfaces, we obtain $\Delta E_f^{B-A} = -1.01$ eV and $\Delta E_f^{C-B} = 0.12$ eV. However, as the polar instability is absent in the superlattice model with two identical interfaces [24], the thickness-dependent polar instability induced energy difference term $\Delta E = E^{chain} - E^{planar}$ [shown in Fig. 2(a)] was simply added to ΔE_f^{C-B}, i.e., $\Delta E_f^{C-B} = 0.12 + \Delta E$. In this vein, we can conclude that the order of relative stability of three interfaces is B > C > A when the thickness of LNO film is more than 2 *uc*, while the order will be C > B > A if the thickness of LNO film is less than 2 *uc*. Notably, type A is always energetically disfavored in any cases. In contrast to the direct process, however, the type A can also be obtained by means of the chemical reduction from type B interface [8,25,26].

D. Electronic structure

Obvious interface reconstructions with respect to bulk materials have been observed to be dependent on interfacial configuration. In this section, we will explore the implications of the interface morphology on the electronic structure.

We will begin with the type A interface, even if it is the most unlikely configuration according to the thermodynamic calculation in Sec. III C. It adopts a G-type AFM order in Ni's layers but an A-type AFM order in Mn's layer, which are both different from their counterparts. The Mn^{3+} in LMO is expected to be in a high spin state ($S = 2$) with $3d^4$ ($t_{2g}^3 e_g^1$)

configuration. However, the magnetic moment of Mn ions at type A interface is about 4.2 μ_B, 10% larger than 3.8 μ_B in bare LMO film on $SrTiO_3$ substrate [27]. This is related with the change of surrounding environment at Mn sites: the Mn ions at type A interface host not an octahedral geometry but a pyramidal one. Compared to the MnO_6 octahedron in LMO, the apical oxygen-free structure (MnO_5 pyramid) results in an electron gain at central Mn sites as demonstrated by the Bader charge results in Fig. 5. More than that, the apical oxygen-free structure results in the decrease of Coulomb repulsion force in the z direction and then a downward shift of the $d_{3z^2-r^2}$ orbital as shown in Fig. 4(a). The relative change of the e_g occupancy is defined as $r = \frac{n_{3z^2-r^2}}{n_{x^2-y^2}} - 1$. In comparison to 3% in bare LMO film on $SrTiO_3$ shown in Fig. 4(d), the
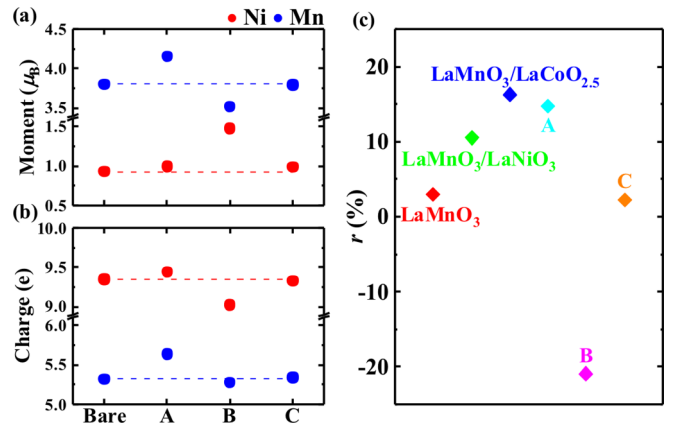

FIG. 5. (a) The magnetic moments and (b) Bader charge analysis results in bare LMO (LNO) thin films or in three LMO/LNO superlattices. (c) The relative change of e_g occupancy r obtained in some previous work [28,29] and in this work.

observed relative change of the Mn e_g occupancy is 15% in type A superlattice, manifesting the strong impact of oxygen coordination manipulation on interface. In a word, this structural transition from MnO_6 to MnO_5 through $NiO_2|La|MnO_2$ interface combination contributes to not only the electron gain at Mn sites, thus the increase of magnetic moment, but also a preferential occupation of the $d_{3z^2-r^2}$ orbital.

For type B interface, the most thermodynamically stable one, the system adopts a C-AFM order in Ni's layers and a FM order in Mn's layer, a simple magnetic ground-state combination of P-LNO and LMO on STO. The magnetic moment of Ni atoms in pyramidal crystal field is $1.4\,\mu_B$, which is significantly larger than $0.9\,\mu_B$ in bare LNO film. As shown in Fig. 4(b), the Ni $d_{3z^2-r^2}$ orbitals are not fully occupied. Compared to the square planar geometry in P-LNO, the Ni atoms at type B interface host a pyramidal geometry. Based on the Bader charge analysis in Fig. 5(b), we find that Ni^{1+} loses some electrons to become $Ni^{1+\delta}$, which in turn makes the spin-down $d_{3z^2-r^2}$ orbitals partially unoccupied. At the same time, the spin state is larger than $1/2$ of Ni^{1+}. So, a great enhancement of Ni magnetic moments is observed at interface. However, no obvious electron gain or loss at Mn sites is observed. Therefore, charge transfer mainly occurs between the apical oxygen and the center nickel. Moreover, the e_g orbitals for the Mn ion located at octahedral site are no longer degenerated, i.e., the $d_{x^2-y^2}$ orbitals are shifting downwards with respect to the $d_{3z^2-r^2}$ orbitals. The relative occupancy change for the Mn ions at type B interface is about -21%, which is significantly larger than -7% in bare LMO films under a large tensile strain [28]. Obviously, this interface presents an alternative way to control orbital reconstructions.

As for the interface of type C, which is thermodynamically stable in ultrathin limit, it is overall FM and metallic. As shown in Figs. 4(c), 5(a), and 5(b), the projected density of states of Ni and Mn e_g orbitals, the magnetic moments and Bader charges of the type C interface are almost the same as those of bulk counterparts. The magnetic moments of Ni are slightly enhanced compared to $0.9\,\mu_B$ in P-LNO, this is due to the stretch along the direction without oxygen chain. This lattice deformation changes the strength of Ni-O-Ni exchange energy and the hybridization between La $5d$ and O $2p$ orbitals. Besides, the Mn-O-Mn bond angle is $149°$, smaller than $157°$ in bare LMO, i.e., the distortion of the oxygen octahedra in LMO is slightly enhanced in C-LNO/LMO superlattice.

In Fig. 5(c) we summarize the orbital preferential occupation in some systems related with LMO. The r of LMO can be tuned from $+4\%$ to -7% under biaxial strain var-

ied from $a = 3.79$ to 4.01 Å [28]. The charge transfer in $LaMnO_3/LaNiO_3$ superlattice results in a $d_{3z^2-r^2}$ preferential occupation with $r = 10\%$ [29]. Now we obtain a large change of Mn e_g occupancy about 15% (-21%) in type A (B) LMO/LNO superlattices. Therefore, we believe that non-isostructural interface design is a promising way for large orbital reconstruction at interface.

IV. SUMMARY

Based on DFT calculations, the transition of ultrathin LNO film from the bulk-planar structure to a chain-type thin film are predicted and the accompanying orbital reconstructions are investigated. The impact of biaxial strain on this transition is also discussed. Considering the substantial changes to electronic structures accompanying this structure transition, three possible interfacial configurations are established for LNO/LMO superlattices. We revealed distinct features that emerge at three different interfaces in the ultrathin limit. A relative orbital occupancy change ratio up to 15% (-21%) is observed at type A (B) heterointerface with preferential occupation of $d_{3z^2-r^2}$ ($d_{x^2-y^2}$) orbitals. In addition, the change of B-site polyhedra caused by asymmetric interface design contribute not only to the orbital reconstruction, but also to the interfacial enhanced magnetic moments of B-site ions located in the center of BO_5 pyramids through charge reconstruction. Our results demonstrate the strong impact of oxygen coordination manipulation based on asymmetric interface design on orbital configurations and electronic properties, providing approaches to explore emergent orbital-driven phenomena.

[1] Y. Tokura and N. Nagaosa, Science **288**, 462 (2000).

[2] D. Li, K. Lee, B. Y. Wang, M. Osada, S. Crossley, H. R. Lee, Y. Cui, Y. Hikita, and H. Y. Hwang, Nature (London) **572**, 624 (2019).

[3] Z. Liao, E. Skoropata, J. W. Freeland, E.-J. Guo, R. Desautels, X. Gao, C. Sohn, A. Rastogi, T. Z. Ward *et al.*, Nat. Commun. **10**, 589 (2019).

[4] J. Zhang, Z. Zhong, X. Guan, X. Shen, J. Zhang, F. Han, H. Zhang, H. Zhang, X. Yan, Q. Zhang *et al.*, Nat. Commun. **9**, 1923 (2018).

[5] J. Chakhalian, J. W. Freeland, H.-U. Habermeier, G. Cristiani, G. Khaliullin, M. van Veenendaal, and B. Keimer, Science **318**, 1114 (2007).

[6] K. R. Poeppelmeier and J. M. Rondinelli, Nat. Chem. **8**, 292 (2016).

[7] E. Dagotto, T. Hotta, and A. Moreo, Phys. Rep. **344**, 1 (2001).

[8] M. A. Hayward, M. A. Green, M. J. Rosseinsky, and J. Sloan, J. Am. Chem. Soc. **121**, 8843 (1999).

[9] D. Kaneko, K. Yamagishi, A. Tsukada, T. Manabe, and M. Naito, Physica C (Amsterdam) **469**, 936 (2009).

[10] Z. Zhong, G. Koster, and P. J. Kelly, Phys. Rev. B **85**, 121411(R) (2012).

[11] P. E. Blöchl, Phys. Rev. B **50**, 17953 (1994).

[12] G. Kresse and J. Furthmüller, Phys. Rev. B **54**, 11169 (1996).

[13] G. Kresse and D. Joubert, Phys. Rev. B **59**, 1758 (1999).

[14] J. P. Perdew, K. Burke, and M. Ernzerhof, Phys. Rev. Lett. **77**, 3865 (1996).

[15] J. P. Perdew, A. Ruzsinszky, G. I. Csonka, O. A. Vydrov, G. E. Scuseria, L. A. Constantin, X. Zhou, and K. Burke, Phys. Rev. Lett. **100**, 136406 (2008).

[16] A. I. Liechtenstein, V. I. Anisimov, and J. Zaanen, Phys. Rev. B **52**, R5467 (1995).

[17] J. H. Park, C. T. Chen, S. W. Cheong, W. Bao, G. Meigs, V. Chakarian, and Y. U. Idzerda, Phys. Rev. Lett. **76**, 4215 (1996).

[18] A. S. Botana and M. R. Norman, Phys. Rev. X **10**, 011024 (2020).

[19] See Supplemental Materials http://link.aps.org/supplemental/10.1103/PhysRevB.104.045310 for details about convergence test for k mesh, magnetic stability, a further analysis of the U dependence, orbital reconstruction in C-LNO films, self-doping effect of La $5d$ bands, formation energy of bulk LMO (LNO) and orbital projected band structures.

[20] K.-W. Lee and W. E. Pickett, Phys. Rev. B **70**, 165109 (2004).

[21] D. Samal, H. Tan, H. Molegraaf, B. Kuiper, W. Siemons, S. Bals, J. Verbeeck, G. Van Tendeloo, Y. Takamura, E. Arenholz *et al.*, Phys. Rev. Lett. **111**, 096102 (2013).

[22] G.-X. Qian, R. M. Martin, and D. J. Chadi, Phys. Rev. B **38**, 7649 (1988).

[23] C. G. Van de Walle, D. B. Laks, G. F. Neumark, and S. T. Pantelides, Phys. Rev. B **47**, 9425 (1993).

[24] H. Chen, A. M. Kolpak, and S. I.-Beigi, Adv. Mater. **22**, 2881 (2010).

[25] M. Crespin, P. Levitz, and L. Gatineau, J. Chem. Soc. Faraday Trans. **79**, 1181 (1983).

[26] M. Kawai, K. Matsumoto, N. Ichikawa, M. Mizumaki, O. Sakata, N. Kawamura, S. Kimura, and Y. Shimakawa, Cryst. Growth Des. **10**, 2044 (2010).

[27] J. B. A. A. Elemans, B. Van Laar, K. R. Van Der Veen, and B. O. Loopstra, J. Solid State Chem. **3**, 238 (1971).

[28] X. Chen, S. Zhang, B. Liu, F. Hu, B. Shen, and J. Sun, Phys. Rev. B **100**, 144413 (2019).

[29] A. T. Lee and M. J. Han, Phys. Rev. B **88**, 035126 (2013).